On the trend in northern hemisphere winter atmospheric circulation during the last half of the 20th century

Jian Lu, Richard J. Greatbatch and K. Andrew Peterson

Department of Oceanography,
Dalhousie University,
Halifax, Nova Scotia, Canada B3H 4J1

Received May 2003; accepted _____

Submitted to *Journal of Climate*

Short title:

Abstract.

During the last half century, the trend in the northern hemisphere tropospheric circulation has been associated with a deepening of both the Aleutian and Icelandic lows, a pattern akin to the "Cold Ocean Warm Land" (COWL) pattern. We use a simplified dynamical model to show that the observed simultaneous deepening trend in both the Aleutian and Icelandic lows can be largely explained as a hemispheric planetary wave response to tropical diabatic forcing in the Indo-Pacific region. In the model, the extra-tropical storm tracks play a role in modulating the wave train, tending to enhance (weaken) the anomalous Icelandic (Aleutian) low in the North Atlantic (North Pacific) sector. The model results also suggest two ways in which the circulation trend over the North Atlantic sector could have been influenced by tropical forcing: one a direct, linear planetary wave response from the eastern tropical Pacific, and the other an indirect response of the North Atlantic storm track to tropical forcing over the western Indo-Pacific region. The possible role of tropical SST warming and anthropogenic forcing is also discussed.

1. Introduction

During the 1970's, there was a well-documented change in the climate system over the Pacific Ocean (e.g. Nitta and Yamada, 1989; Trenberth and Hurrell, 1994; Mantua et al., 1997; Trenberth et al., 1998; Trenberth et al., 2002). In particular, there was an abrupt rise in tropical Pacific sea surface temperature (SST) that took place around 1976-77. At about the same time, there was a deepening of the Aleutian low leading to stronger westerly winds around $40°N$ and an associated enhanced surface heat loss leading to cooler underlying SST. These changes are indicative of the tendency for the positive polarity of the Pacific-North America (PNA) pattern (Wallace and Gutzler, 1981) to predominate since the 1970's. Meanwhile, El Niño events have become more frequent and persistent since the 1970's, and there has also been a change in the way El Niño events evolve (Wang, 1995; Wang and An, 2001; Trenberth and Hoar, 1996; Trenberth et al., 2002).

Wintertime climate over the Euro-Atlantic region also underwent a change during the 1970's. The North Atlantic Oscillation (NAO), the primary mode of variability in the northern hemisphere winter atmospheric circulation, showed a strong upward trend in its index that began during the 1970's (Hurrell, 1995; Hurrell, 1996) and lasted until at least the mid-1990's. In addition, the spatial pattern associated with the interannual variability of the NAO shifted eastward during the period 1978-97 compared to 1958-97 (Hilmer and Jung, 2000), resulting in a strong link between the NAO and ice export through Fram Strait during 1978-97 that did not exist during 1958-77. Our previous studies (Lu and Greatbatch, 2002; Peterson et al., 2003) have linked the eastward shift of the NAO to the enhanced eddy-mean flow interaction initiated by the increase in baroclinicity at the upstream end of the North Atlantic storm track in association with positive NAO index. Based on this mechanism, the recent shift in the spatial pattern of the NAO can be attributed to the relatively high NAO index during the 80's and 90's versus the relatively low index during the 60's and 70's. Related to the upward trend in

the NAO, Christensen(2003) has noted a regime shift in the winter stratospheric polar vortex with the strong polar vortex state being occupied in preference to the weak polar vortex state since the 1970's. It has also been noted that much of the warming over the northern hemisphere during winter since the 1970's can be linked to the upward trend in the NAO (Hurrell, 1996) and the related Arctic Oscillation (AO) index (Thompson et al., 2000). There has also been considerable speculation that the upward trend in the NAO/AO may be anthropogenically driven (see Gillett et al., 2003, for a review).

It has been suggested that both the changes in the PNA and the NAO noted above have been driven by forcing from the tropics. In the case of the PNA, influence of tropical Pacific SST is well established (see Trenberth et al., 1998, for a review). In particular, warming of the tropical Pacific, such as took place during the 1970's, is known to drive a tendency for a deepened Aleutian low like that observed (e.g. Graham, 1994; Lau and Nath, 1994; Lau and Nath, 1996; Lau, 1997). The recent paper by Newman et al.(2003) goes further and suggests that climate change over the North Pacific is driven by the El Nino/Southern Oscillation (ENSO) phenomenon and, by implication, attributes the 1970's transition in the atmospheric circulation over the North Pacific to the change in the character of the ENSO index that took place around 1976-77. More problematic is how tropical forcing (e.g. associated with SST anomalies) can affect the North Atlantic sector. In our previous studies (Peterson et al., 2002; Greatbatch et al., 2003), we used a simple, dynamical model of the atmosphere, driven by forcing derived from observations, to successfully hindcast the observed winter NAO index for the period 1949-99. By allowing the forcing to vary from year to year only in the tropics, or only in the extra-tropics, we showed that the recent upward trend in the NAO is related to tropical forcing, whereas, by corollary, the coupling with the mid-latitude or Arctic Ocean is not important for the trend. This result agrees with the work of Hoerling et al.(2001), where evidence is presented that North Atlantic climate change since 1950 is linked to a progressive warming of tropical SST. In addition, Hoerling et al. also showed

that the tropospheric response to the gradual tropical ocean warming manifests itself in the NCAR CCM3 model as a trend with a spatial structure like that of the NAO over the North Atlantic and the PNA over the North Pacific, very much like the observed trend (Fig.1a). Such a hemispheric structure bears a strong resemblance to the "Cold Ocean Warm Land" (COWL[1]) pattern of Wallace et al. (1995, 1996) (see Fig.1b), an issue discussed further in Section 3. The important role played by the COWL pattern in recent climate change has also been noted by Corti et al.(1999). As can be seen from Fig.1b, variations in the COWL index are associated with synchronous deepening of the Aleutian and Icelandic lows (in contrast to variations in the AO index which are associated with out of phase variations of the Aleutian and Icelandic lows).

In this paper, following the methodology of Peterson et al. (2002, 2003) and Greatbatch et al. (2003), we use a simple, dynamical model to investigate the trend in the boreal winter tropospheric circulation. The model, originally introduced by Hall (2000), is driven by forcing derived from observations and is used in this study as a diagnostic tool. We wish, in particular, to investigate the driving mechanism for the atmospheric circulation trend and the relationship between the extratropical response and the tropical forcing. The model details and the data used for the diagnostics are presented in Section 2. Before embarking on the model experiments, a Singular Value Decomposition (SVD) analysis is carried out in Section 3 in order to identify the tropical forcing for the model that accounts for the tropospheric circulation trend in a linear covariance sense. A spatial analysis is then performed on the circulation patterns related

[1]The COWL index is defined as a weighted average of winter mean 1000-500 hPa thickness north of $40°N$, with a positive, uniform weight over the land and a negative, uniform weight over the ocean, the sum of the weights adding to zero. The COWL pattern, shown in Fig.1b, is obtained by regression of the winter mean 500 hPa height against the COWL index.

to the multidecadal climate change, including the pattern associated with the first two SVD modes and the AO. As the core of this study, Section 4 presents the results of a suit of experiments using both the full nonlinear model and its linearized version. These results point to the importance of tropical, especially the Indo-Pacific diabatic forcing, in driving the trend in both the North Pacific and North Atlantic sectors, and the importance of a planetary wave train in communicating the information about tropical changes to the Euro-Atlantic sector. Finally, the results of this study are summarized in Section 5, where we also discuss some remaining questions and challenges.

2. Data and Methodology

a. Data

The NCAR/NCEP reanalysis (Kistler et al. 2001) is the main data source used in this study. Daily mean data from the NCAR/NCEP reanalysis are used to diagnose the model forcing as well as for model initialization. The period of analysis spans 51 winters (December 1st to February 28) from 1948/49 to 1998/99 (a total of 4590 daily realizations) and the forcing is calculated for each winter separately. To feed the data into the model, horizontal velocity, temperature and geopotential height are linearly interpolated to the model's Gaussian grid and the 5 σ levels. Sea level pressure (SLP) is calculated by integration of the barometric equation from the 1000 mb height to zero (sea level) using the 1000 mb temperature and 1000mb height products from the NCAR/NCEP reanalysis.

In order to directly compare with Hoerling et al. (2001), we use the 500 hPa height field to represent the tropospheric circulation. Thus, wintertime 500 hPa height data from NCAR/NCEP is extensively employed not only in terms of mean circulation but also transient eddy activity at the 500 hPa level. We also make use of the NCAR/NCEP SST product for winters from 1948/49 to 1998/99.

b. The Hall model

The model employed here is the dry, primitive equation model for the atmosphere described by Hall (2000) (hereafter the Hall model). The model equations are written in terms of vorticity, divergence, temperature and surface pressure and are solved spectrally with a horizontal resolution of T21 (approximately 5.625° in latitude and longitude) on 5 equally spaced σ levels, the core code being that described by Hoskins and Simmons (1975). The model has linear damping and is run with time-independent forcing computed from observations. Here we use the daily mean data from the NCAR/NCEP reanalysis to compute the forcing separately for each of the 51 winters from 1949 to 1999. The specification of the damping and model parameters is exactly as in Hall (2000). The Hall model is computationally very efficient, enabling many, large-member ensembles of model experiments to be conducted.

For simplicity, following the convention of Hall (2000), the equation describing the model's evolution with time can be written as

$$\frac{\partial \mathbf{\Psi}}{\partial t} = N(\mathbf{\Psi}) + \mathbf{f}, \tag{1}$$

where $\mathbf{\Psi}$ represents the model variables and $N(\mathbf{\Psi})$ all the nonlinear terms and the damping (the damping terms are specified in a linear form). $\mathbf{f}$ is the forcing term, which, in this study, is time independent. To derive the forcing, a statistical equilibrium state is assumed in each winter. We do a time average and form the time-mean budget equation by splitting $\mathbf{\Psi}$ into a long-time mean $\overline{\mathbf{\Psi}}$ and an instantaneous perturbation $\mathbf{\Psi}'$. Thus

$$\overline{\frac{\partial \mathbf{\Psi}}{\partial t}} = \overline{N(\mathbf{\Psi})} + \mathbf{f}, \tag{2}$$

where

$$\overline{N(\mathbf{\Psi})} = N(\overline{\mathbf{\Psi}}) + \overline{E(\mathbf{\Psi}')}. \tag{3}$$

As shown by (3), nonlinearity in the model can be divided into parts associated with the mean state $\overline{\mathbf{\Psi}}$ and eddy flux $\overline{E(\mathbf{\Psi}')}$. Assuming a statistical equilibrium, the average

of the time derivative term over the averaging period is small in amplitude compared to the individual terms on the right hand side, and the $\overline{\frac{\partial \mathbf{\Psi}}{\partial t}}$ term on the left hand side of equation (2) can be approximated to be zero. This leaves a balance between $\overline{N(\mathbf{\Psi})}$ and $\mathbf{f}$, i.e.,

$$\mathbf{f} = -\overline{N(\mathbf{\Psi})} \tag{4}$$

or, using (3),

$$-N(\overline{\mathbf{\Psi}}) = \mathbf{f} + \overline{E(\mathbf{\Psi}')}. \tag{5}$$

This, as one expects, turns out to be a good approximation for the solstice seasons. Inserting the observed atmospheric states (denoted by $\mathbf{\Phi}$) into (4) in place of $\mathbf{\Psi}$, a time-independent model forcing $\mathbf{f}$ is obtained in terms of the action of the nonlinear operator N on the observed states $\mathbf{\Phi}$, i.e., $\mathbf{f} = -\overline{N(\mathbf{\Phi})}$ (see eqn. (7)). Here, $\mathbf{f}$ is calculated using daily mean observed states $\mathbf{\Phi}$. Likewise, replacing $\mathbf{\Psi}$ in (5) with $\mathbf{\Phi}$, the left hand side, $-N(\overline{\mathbf{\Phi}})$ represents the maintenance of the time-mean state $\overline{\mathbf{\Phi}}$ against its own advective tendencies and against damping. $-N(\overline{\mathbf{\Phi}})$ has two contributions, one from the forcing $\mathbf{f}$ and the other from the transient-eddy flux convergence $\overline{E(\mathbf{\Phi}')}$. The second term, $\overline{E(\mathbf{\Phi}')}$, often dubbed the "transient-eddy forcing", represents the effect of the observed transient fluxes in the time-mean budget. This "eddy forcing" can be derived by subtracting the "diabatic forcing" $\mathbf{f}$ from $-N(\overline{\mathbf{\Phi}})$, i.e., $\overline{E(\mathbf{\Phi}')} = -N(\overline{\mathbf{\Phi}}) - \mathbf{f}$.

We now outline the method of computing the forcing from the data. The effect of the N operator on any initial condition $\mathbf{\Psi_0}$ can be found by running the model without forcing for one time step, giving the instantaneous tendency

$$(\frac{\partial \mathbf{\Psi}}{\partial t})_{unf} \approx \frac{\mathbf{\Psi}^{+}_{unf} - \mathbf{\Psi_0}}{\delta t} = N(\mathbf{\Psi_0}) \tag{6}$$

where the subscript unf denotes an unforced integration of the model and the superscript $+$ refers to the state after one time step. The time step of integration is δt. Thus, using (4), $\overline{N(\mathbf{\Phi})}$ can be found by averaging the result of setting $\mathbf{\Psi_0} = \mathbf{\Phi_i}$, where

subscript $\mathbf{i}$ identifies one realization of $\mathbf{\Phi}$ among n observations. Thus

$$\mathbf{f} = -\overline{N(\mathbf{\Phi})} = -\frac{1}{n\delta t}\sum_{\mathbf{i}=1}^{n}\{\mathbf{\Psi}^{+}_{\mathbf{i}unf} - \mathbf{\Phi_i}\} \tag{7}$$

Likewise, $-N(\overline{\mathbf{\Phi_c}})$ can be found by setting $\mathbf{\Psi_0} = \overline{\mathbf{\Phi_c}}$ without stepping through the entire time series of data. Thus,

$$-N(\overline{\mathbf{\Phi_c}}) = -\frac{\mathbf{\Psi}^{+}_{unf} - \overline{\mathbf{\Phi_c}}}{\delta t} \tag{8}$$

The model forcing calculated using (7) mimicks processes not explicitly included in the model code, most importantly the diabatic forcing of the atmosphere due to incoming solar radiation, latent and sensible heat release associated with deep convection and the midlatitude storm track (Hoskins and Valdes, 1990), and since the model has a flat bottom, the effect of the missing orography. Diagnosing forcing from observations, as we do here, eliminates some of the uncertainty in the way fully interactive AGCM's compute diabatic heating, for example in response to SST forcing in the tropics. When the model is driven by forcing $\mathbf{f}$, as in our nonlinear model experiments, the model must develop its own transient-eddy activity. The forcing associated with this transient activity, $\overline{E(\mathbf{\Psi}')}$, must agree with $\overline{E(\mathbf{\Phi}')}$ if the model is to reproduce the observed mean state, $\overline{\mathbf{\Phi}}$ (as is the case in all the model experiments described here). For the purpose of convenience, the forcing $\mathbf{f}$ will be referred to as "diabatic" forcing in this paper.

We now explain more about the linearized version of the Hall model. Specifying the model state as $\mathbf{\Psi} = \overline{\mathbf{\Phi_c}} + \mathbf{\Psi_p}$, where $\mathbf{\Psi_p}$ is a small perturbation to the background state, $\overline{\mathbf{\Phi_c}}$, and setting the forcing $\mathbf{g} = -N(\overline{\mathbf{\Phi_c}}) + \mathbf{g}'$, where $-N(\overline{\mathbf{\Phi_c}})$ is used as the forcing to maintain the background state and $\mathbf{g}'$ is a small perturbation, the model equation becomes

$$\frac{\partial \mathbf{\Psi_p}}{\partial t} = \mathbf{L}_{\overline{\mathbf{\Phi_c}}}(\mathbf{\Psi_p}) + \mathbf{g}', \tag{9}$$

where, $\mathbf{L}_{\overline{\mathbf{\Phi_c}}}$ is a linear operator that depends on the background state, $\overline{\mathbf{\Phi_c}}$, about which the model is linearized, and terms of quadratic or higher order in perturbation amplitude

have been neglected. Thus (9) is the associated time-dependent linear perturbation model. In practise, the full nonlinear model code is used and the perturbation, $\mathbf{g}'$, to the forcing $-N(\overline{\mathbf{\Phi_c}})$ is chosen to be sufficiently small that (9) remains a good approximation during the period of integration (see Section 4a for further details). This linearization technique has been used before by Hall and Sardeshmukh (1998) to examine the first eigenmode of $\mathbf{L}$ of the climatological mean circulation, and by Jin and Hoskins (1995) to study the direct response to a perturbation in tropical forcing.

3. SVD and Spatial Analysis

a. SVD analysis

Prior to embarking on the model experiments, we first conduct a SVD analysis to shed some light on the relationship between the model forcing and the observed atmospheric circulation. SVD is a technique to isolate spatial patterns in two fields that tend to occur synchronously with one another (and hence explain maximum covariance between the two fields) and could be physically related to each other by some linear dynamics. The readers are directed to Bretherton et al. (1992) for the details of SVD techniques and Wallace et al.(1992) for an application to sea surface temperature and 500 hPa height over the Pacific.

Here, an SVD analysis is applied to the vertically-integrated forcing for the temperature equation (left field) over the tropical Indo-Pacific region ($40°S$-$40°N$, $60°E$-$60°W$, see Fig.2b) and mean 500 hPa height fields (right field) over the northern hemisphere ($20°$-$80°N$) for each of the winters 1949-99[2]. The first SVD mode (hereafter SVD1) explains 50% of covariance (in terms of squared covariance fraction, SCF,

[2]SVD analysis applied to the model forcing for the divergence or vorticity equations and 500 hPa height fields yields almost identical temporal and 500 hPa height structure for the leading SVD mode.

computed as explained in Bretherton et al., 1992) between these two fields and the correlation between the first pair of extension coefficients is 0.76. The extension coefficients for the left (500 hPa height) and right (forcing) vectors are denoted by a(t) and b(t) respectively in Fig.2c. Time series b(t) features an upward transition that occurred in the late 70's, indicating a "regime shift" as observed in other climate indices and as discussed in the introduction. To gain more confidence in the link between the leading pair of SVD vectors, a companion empirical orthogonal function (EOF) analysis was carried out on both fields separately. The first EOF of diabatic forcing is almost identical to the first right singular vector (Fig.2b) and its principle component time series (PC) is significantly (at 1% confidence level) correlated (r=0.52) with the PC of the second 500 hPa height EOF, which itself is spatially correlated at 0.81 with the pattern of the 500 hPa height trend (Fig.1a) and at 0.85 with the pattern of the left singular vector shown in Fig.2a.

The first SVD left singular vector (Fig.2a) and the observed trend in 500 hPa height (see Fig.1a) are almost identical to each other, being spatially correlated at 0.96, suggesting that the SVD analysis picks out the tropical diabatic forcing that is intimately related to the trend. This diabatic forcing pattern (Fig.2b) is characterized by a band of enhanced heating south of the equator spanning the Indian Ocean to the tropical South Pacific Ocean, and a cooling over the western and central subtropical North Pacific. Given the fact that the tropical diabatic forcing is dominated by latent heat release associated with convective precipitation, the diabatic forcing pattern revealed by the first SVD is likely to be related to precipitation anomalies associated with the variations in tropical SST. Indeed, the diabatic forcing shown in Fig.2b does share some common features with the precipitation trend in Figure 4 of Hoerling et al. (2001) driven by tropical SST in their TOGA experiment. Also, the major dipole feature over the central tropical Pacific bears a strong resemblance to that in the composite of anomalous OLR (outgoing longwave radiation) shown in Figure 18 of Trenberth and

Hurrell (1994) for years with a deeper than normal Aleutian low.

To investigate further the connection with tropical SST, Fig.2d shows the SST pattern obtained by regressing the 51 winter mean SST against the time series of b(t). This gives rise to a pattern almost the same as that of the SST trend shown in Manabe et al.(2001) (see also Knutson and Manabe, 1998) and in McPhaden and Zhang(2002). These latter authors note the connection between the warming trend in the eastern equatorial Pacific and the trend towards westerly wind anomalies over the tropical Pacific (see also Wang and An, 2001; 2002).

Besides the close relationship to the trend and the second EOF of 500 hPa height field, the first SVD mode also has a connection to the COWL pattern (cf. Figs. 2a and 1b) and the leading EOF mode of northern hemispheric storm activity (NHST1) introduced by Chang and Fu (2002). This can be seen in Fig.3 by comparing a(t), i.e., the SVD1 expansion coefficient for 500 hPa height (bottom, also shown as a dashed line in Fig.2c) with the time series of the COWL index (middle) and the PC of NHST1 (top). Like the time series a(t) associated with the first SVD mode, the first PC time series of Chang and Fu shows a conspicuous upward transition during the 1970's, and is associated with an increase in storm activity over both the North Atlantic and North Pacific basins. In fact, each of the three curves experiences a transition-like increase during the 1970's and all are significantly correlated with each other at or better than the 1% level. In fact, 50% of the covariance between NHST1 and a(t) can be explained reciprocally, with half of the covariance being accounted for by the upward transition during the 1970's and half due to coherency on interannual time scales, as revealed by comparing their detrended and non-detrended cross correlations. On the other hand, the high correlation between the COWL index and a(t) comes not from the trend, but rather from their congruent evolution on interannual time scales, as can be inferred from the slightly increased correlation for the detrended versus the nondetrended time series.

Although COWL was first defined in terms of the thermal contrast between ocean

and continent (Wallace et al., 1996), the circulation pattern associated with the positive COWL index appears to be a preferred circulation regime when viewed from a nonlinear dynamical perpective. This is because the positive COWL circulation regime emerges naturally from nonlinear regime extraction techniques, such as clustering analysis (e.g. Palmer, 1999; Corti et al., 1999) or nonlinear principle component analysis (Monahan et al., 2001). Furthermore, the positive COWL pattern can be replicated by a low-order model as an equilibrium state in a hyperspace spanned by the leading EOF's of the reference GCM (D'Andrea, 2002). Similar to the NAO and AO, COWL is a climate variability mode internal to the climate system, and its existence does not depend on dynamical air-sea coupling or external radiative forcing (Wallace et al., 1995; Broccoli et al., 1998), but rather on the land-ocean contrast imposed by the geography. The high correlation between the COWL index and the leading SVD expansion coefficients (correlation coefficient equals 0.76 with a(t), and 0.43 with b(t)) hints at an important influence of tropical forcing on the COWL mode. It has been suggested that tropical Pacific SST warming can impact the frequency with which the COWL regime is occupied (Palmer, 1999), leading to a significant impact on northern hemispheric temperature (Kumar and Hoerling, 1998). The dynamical link between tropical forcing and the recent COWL-like circulation trend is explored further in Section 4.

b. Spatial analysis

Having seen the temporal coherency between the first SVD mode and the COWL and NHST1 modes, we generated the 500 hPa patterns associated with COWL and NHST1 by regressing winter mean 500 hPa height data against the corresponding standardized indices, and then projecting them, as well as the patterns of the trend and the leading two left singular vectors, onto the first two EOF's of the northern hemisphere (20°-80°N) winter mean 500 hPa height fields. All the patterns have been normalized by the area-weighted standard deviation of their spatial variance on the grid used for

the analysis (in this case, 2.5° in latitude by 5° in longitude). The results are shown in Fig.4. The leading two EOF's, consistent with others (Kimoto and Ghil, 1993; Corti et al., 1999), are 500 hPa versions of the AO (first EOF) and PNA (second EOF). Each pattern is plotted as a colored line in Fig.4 with the end point defined by the projection coefficients of the pattern on both EOF's. The length of the line represents the extent to which the pattern can be expressed by the leading two EOF's, and the angle from the axes indicates the relative spatial similarity of the patterns to the EOF's. Consistent with the temporal analysis, the patterns associated with the tropical diabatic heating source (SVD1, magenta), with northern hemisphere storm track activity (NHST1 mode, green), and with the land-ocean thermal contrast (COWL, cyan) all cluster around the trend pattern (red), indicative of their linkage to the circulation trend during 1949-99. The 500 hPa patterns of the leading two SVD modes are coincidently parallel to the leading two EOF's of 500 hPa height, but with the order of the modes reversed in the SVD analysis due to the selection of a COWL-like pattern by the model tropical forcing. Note that the COWL-like pattern is basically a PNA teleconnection wave train over the North Pacific and neighbouring continents, but with an NAO-like tail extending to the North Atlantic region.

EOF1 here represents the AO on the 500 hPa height surface, being depicted as the abscissa in the EOF coordinate and nearly orthogonal to the "COWL-like" cluster. The orthogonality between the AO and the "COWL-like" trend indicates the limitation of the AO in portraying the circulation trend since the middle of the 20th century. Indeed Fig.4 suggests that COWL may be a better paradigm through which to understand recent circulation changes than the AO (see also Corti et al., 1999).

4. Model experiments

a. Design of the experiments

Table 1 summarizes the model experiments. First, in order to substantiate the dynamical link between the first pair of singular vectors obtained from the SVD analysis, we regress the model forcing for all the model equations over the global domain against the time series b(t) and apply the resultant forcing, which we call SVD1 forcing, to the linearized version of the Hall model. In all the linear experiments, the model is linearized about the observed mean state obtained by averaging over all the 51 winters. In the linearized model, this mean state is balanced by a forcing (containing both "diabatic" and "eddy" effects) calculated using equation (8) and which we call the "mean state" forcing. The SVD1 forcing, as a perturbation forcing, is then added to the "mean state" forcing after being weighted by 0.1 (the solutions will be scaled back to the proper amplitude for presentation). This small weighting keeps the perturbative part of the response small and delays the triggering of baroclinic instability. Each experiment uses the same initial condition, i.e. the climatological mean state for all 51 winters, and is run for 30 days. The model results are averages from day 10 to 16, before baroclinic instability sets in (Jin and Hoskins, 1995). The model response within this time consists of quasi-stationary planetary waves, in a medium of realistic background flow, and maintained by the SVD1 forcing.

Six sets of linear experiments were carried out by specifying the SVD1 forcing over the globe (**L_G**), the tropics ($36^\circ S \leq \theta \leq 36^\circ N$, **L_TR**), the extratropics ($\theta > 36^\circ N$, and, $\theta < 36^\circ S$, **L_ET**), the Indo-Pacific region (the region shown in Fig.2b, **L_IP**), the western Indo-Pacific region (that part of the Indo-Pacific region west of the date line, **L_WIP**) and the eastern Pacific (that part of the Indo-Pacific region east of the date line, **L_EP**), where here θ is latitude. In all cases, the method for restricting the forcing to a limited area of the globe follows Greatbatch et al. (2003).

To see what role nonlinearity plays in the dynamics of the trend, some companion experiments have also been conducted with the nonlinear Hall model using the same SVD1 forcing as the corresponding linear counterparts, but this time, added to the average of the 51 "diabatic" forcings calculated for each winter using equation (7). For the global (**N_G**) and tropical (**N_TR**) forcing cases, an ensemble of experiments was carried out for each specified strength of the SVD1 forcing from -1.6 to $+1.6$ at an increment of 0.2. (Recall that the SVD1 forcing is obtained by regression against the time series b(t) in Fig.2c, so that a given specified amplitude of the forcing corresponds to a value of b(t) in the figure.) For the case with the SVD1 forcing imposed only over the western Indo-Pacific region (**N_WIP**), only two ensembles were carried out using a forcing strength of $+1$ and -1, respectively.

The SVD1 forcing is one component of the total forcing. Other factors may also play a role in determining the trend in 500 hPa circulation. For example, the forcing has interannual variability, the response to which may project on the trend through a rectification mechanism (see the discussion in subsection d). Also, the mean states in each winter provide different background states for the SVD1 forcing to act upon, an effect not taken into consideration in the linear experiments described above. Thus, to take account of these other factors, we also run the nonlinear model with the full 51-winter history of the global and tropical forcing in two supplementary ensembles of experiments, these being referred to as **F_G** and **F_TR**, respectively, in Table 1.

In all the nonlinear ensemble experiments mentioned above, each ensemble consists of 30 ensemble members. The ensemble members differ only in the choice of initial conditions, these being chosen randomly from the 4550 winter daily realizations in the NCAR/NCEP reanalysis. Each ensemble member is integrated for 4 months and the analysis is carried out on the final 3 months.

b. Linear experiments

The 500 hPa response in each of the linear model experiments is shown in Fig.5. The amplitude shown in the figures corresponds to one standard deviation of the time series b(t) shown in Fig.2c and can be compared directly with the amplitude of the left singular vector shown in Fig.2a.

We begin with Experiment **L_G**, that is the 500 hPa response to globally specified SVD1 forcing. Given that the correlation between the expansion coefficients going along with the singular vectors is only 0.76 (not 1), it is possible that the model might not reproduce the left vector shown in Fig.2a. Nevertheless, the model does capture most of the features of the left SVD1 vector, e.g. the deepening trend of the Aleutian low, the upward trend of geopotential height over western North America and Europe, and the downward trend in geopotential height over the Greenland and Siberia. The spatial correlation between Fig.5a and Fig.2a is 0.59, which is remarkably high considering that it is estimated over 1800 grids between $20°N$ and $80°N$ over the whole northern hemisphere. Perhaps the most significant deficiency of the linear model is the exaggeration of the positive height anomaly extending from Northern Europe northward to the Barents Sea, although this tendency is also present in the observations.

When only the tropical portion of the SVD1 forcing is used to drive the model (Experiment **L_TR**; see Fig.5b), we immediately see the importance of a hemispheric wave train which emanates from the central and western tropical Pacific and ends over the North Atlantic and Western Europe. The particular arrangement of highs and lows gives rise to a strong projection on to the SVD1 left vector shown in Fig.2a, the spatial correlation being 0.67. The strong similarity of the model-driven pattern to the one derived from SVD analysis indicates a genuine, dynamical connection between the tropical SVD1 forcing (Fig.2b) and the SVD1 left vector for 500 hPa height (Fig.2a). Extratropical forcing, on the other hand, makes almost no contribution to the observed trend (shown in Fig.5c, its spatial correlation with Fig.2a is only -0.01), except for

driving the downward trend in geopotential height near Siberia. The extratropical forcing does, nevertheless, appear to counteract the North Pacific part of the wave train generated by the tropical forcing, as can be seen by comparing the arrangement of highs and lows over the Pacific sector in Figs. 5b and c.

These linear results corroborate the notion of Hoerling et al. (2001) that the trend in 500 hPa height during the past half century originates from the tropics. It is also worth noting that our linear experiments are reasonably successful at capturing the amplitude of the first SVD mode of 500 hPa height, as can be seen by comparing Figs. 5a,b with Fig.2a. (We note in passing that the tropically driven downward trend in geopotential height over the North Atlantic is weaker and displaced southward compared to the observations (Fig.2a), an issue left for investigation in subsection c.) In this sense, our results differ from those of Hoerling et al. (2001). These authors found that the NCAR CCM3 model can only account for half the amplitude of the observed trend when driven by the time series of observed tropical and/or global SST and sea ice. In a more recent paper, Hurrell et al. (2003) argue that the difference can be accounted for by the internal variability of the atmospheric circulation, an issue we shall return to in Section 5.

It is of great interest to know from which part of the tropics the linear wave train originates. Seeing the particular configuration of the planetary wave in Fig.5b, it is conceivable that the wave stems from the tropical Indo-Pacific region. To verify this, we conducted another experiment (**L_IP**) with the SVD1 forcing specified only within the Indo-Pacific region ($40°S$-$40°N$, $60°E$-$60°W$). The results are presented in Fig.5d. Comparing with the linear response to the forcing specified over the whole tropical band (Fig.5b), we can see that the wave train signal is largely reproduced by the Indo-Pacific forcing alone. As another test, an experiment with the SVD1 forcing specified only over the tropical Atlantic region was carried out and shows only a very weak signal at mid-latitudes, and no significant contribution to the wave train seen in Figs. 5b,d

(result not shown). It follows that the forcing for the trend does not originate from the tropical Atlantic, but rather from the tropical Indo-Pacific region, in agreement with Hoerling et al.(2001)'s conclusions.

To further pinpoint which portion or portions of the tropical forcing is related to the wave signal over the North Pacific and/or North Atlantic, two additional linear experiments were performed with the forcing imposed over subregions of the tropics: the western Indo-Pacific ($60°E$-$180°W$, Experiment **L_WIP**) and the eastern Pacific ($180°W$-$60°W$, Experiment **L_EP**). The result of **L_WIP** clearly shows that the PNA-like wave train over the Pacific sector is driven from the western tropical Indo-Pacific (Fig.5e), whereas, the forcing from the eastern tropical Pacific is responsible for the changes over the North Atlantic (Fig. 5f). Thus, in the context of our linear model, the forcing over both the western Indo-Pacific and the eastern Pacific are important for the extratropical circulation trend. Moreover, the relationship between the location of forcing region and the maximum extratropical response is quite consistent with that shown by Simmons et al.(1983). Based on the model evidence gathered thus far, we argue that an atmospheric planetary wave excited by diabatic processes over the tropical Indo-Pacific region communicates the tropical signal to the extratropics including the North Atlantic basin, resulting in COWL-like circulation anomalies similar to the observed trend. Broadly, the change over the North Pacific (near the Aleutian Islands) mostly stems from the western tropical Pacific and Indian Ocean, and the change over the North Atlantic can be mostly attributed to the forcing from eastern half of the tropical Pacific domain. We note, however, that these conclusions are based on the results from the linear model.

c. Nonlinear experiments

The linear model experiments have confirmed the importance of tropical forcing that was first pointed out by Hoerling et al. (2001). Here we begin by focusing on the

nonlinear response to the tropically specified SVD1 forcing (Experiment **N_TR** in Table 1). A 30 member ensemble of experiments was carried out for each specified strength of the tropical SVD1 forcing, the specified strength increasing from -1.6 to $+1.6$ at an increment of 0.2 (implying that there are 17 ensembles of 30 members each, each member differing only in its initial condition). Fig.6a presents the linear trend of the ensemble mean 500 hPa height derived from the 17 different ensembles. To facilitate comparison of magnitude with Fig.5b, the pattern shown in Fig.6a has been rescaled to correspond to 1 standard deviation of the SVD1 time series b(t). Despite a marked modification due to the model nonlinearity, a standing wave train reminiscent of its linear counterpart (Fig.5b) is still discernable over eastern Asia, the North Pacific and North America, but with the North Pacific lobe much damped and shifted poleward. Downstream over the North Atlantic, a pronounced dipole is fully developed and has a strong projection on to the NAO. These differences from the linear result are due to the local effects of model-generated eddies, which, as we demonstrate later, tend to damp (reinforce) the original signal of the linear wave train over the North Pacific (North Atlantic). Incorporating the extratropical portion of the SVD1 forcing to drive the ensembles of experiments (Expt. **N_G**) does not bring any substantial improvement (Fig.6b), except for capturing the downward trend in geopotential height over the central Eurasian continent (although it is southward displaced comparing to the observations). In the meantime the signal near the Aleutian Islands and the Bering Sea in Fig.6a has become merged with that over the North Atlantic to form a region with a downward trend in geopotential height over the whole of the Arctic Ocean.

In a recent paper, Hoerling et al. (2003) ran an ensemble of experiments using the NCAR CCM3 model in which the linear trend in tropical SST (between 25^oS and 25^oN) is imposed at the lower boundary. By restricting the SST forcing to the trend alone (the interannual variability in SST was excluded), Hoerling et al.'s experiments are similar in strategy to ours, in that our set of nonlinear ensembles (Experiment **N_TR**) is driven

by what is essentially the trend in the model tropical forcing. It is therefore of interest to compare the trend shown in Fig.6a with that found by Hoerling et al. (2003; see the upper panels of their Figure 4). Both patterns show an NAO-like dipole over the North Atlantic, corresponding to a trend towards positive NAO index. However, the 500 hPa response over the North Pacific to the SST trend found by Hoerling et al. (2003) shows a trend towards higher geopotential height, in contrast to the observed trend towards lower geopotential height (Fig.1a) and our experiments (Fig.6a) which show a downward trend in geopotential height over the Aleutian Islands and the Bering Sea (although this is displaced poleward compared to the observations). The different behaviour of the Hall model might be related to the fact the diabatic forcing used by the Hall model has a strong loading over the central and eastern tropical Pacific (e.g. Fig.2b) [3], a signal missing in the precipitation response to the trend of tropical SSTs found by Hoerling et al. (2003; see the lower panels of their Figure 4). Indeed, when only the western portion of the Indo-Pacific SVD1 forcing is specified to drive the nonlinear Hall model (i.e., Expt. **N_WIP**), the trend over the North Pacific is characterized by a rise in geopotential height (see Fig.11 and the discussion in Section 5). When driven by the complete monthly history of global or tropical SSTs, the NCAR CCM3 model does produce pronounced rainfall over the central and eastern Pacific and then captures the deepening trend of the Aleutian low (Hoerling et al., 2001, 2003).

To better understand the nonlinear experiments and, in particular, the role of eddy/mean flow interaction, we now look at two of the tropically driven ensembles in more detail, namely those with the SVD1 forcing strength set to -1 and $+1$. Fig.7a,b shows the departure, in each case, of the ensemble mean 500 hPa height from that in the zero SVD1 forcing case. For the purpose of comparison with Fig.5b (the

[3] A similar feature is found in differences of precipitation and cloudiness data between pre- and post- 1976 epochs by Deser et al. (2003); see their Figure 12.

corresponding linear result), the field plotted in Fig.7a has been multiplied by -1 and so has the opposite sign to the actual model response. We can see that the -1 SVD1 forcing case (Fig.7a) is quite similar to the linear model response, whereas there is a marked difference over the North Pacific in the $+1$ SVD1 forcing case shown in Fig.7b, indicating strongly nonlinear behaviour over the North Pacific. By contrast, over the North Atlantic, the original wave signal is enhanced in both -1 and $+1$ cases. To understand the role of transient eddies associated with the storm track, we diagnosed the eddy forcing for the -1 and $+1$ cases by subtracting the "diabatic" only forcing used to drive the nonlinear model from the "diabatic" plus "eddy" forcing calculated using equation (8), and then applying the resultant eddy forcing to drive the Hall model linearized about the mean state for all 51 winters. The respective linear response in 500 hPa height in the -1 and $+1$ cases is shown in Figs.7c and 7d, the former, as before, being the opposite of the actual model response. We see that in both cases, the eddy forcing enhances the linear wave response over the North Atlantic, whereas over the North Pacific the eddy forcing tends to support the linear wave signal in the -1 SVD1 forcing case, but to strongly oppose the linear wave signal in the $+1$ SVD1 forcing case (as indicated by the large positive anomaly centered in the region of the Aleutian low in Fig.7d).

To further clarify the nonlinear behaviour in the model ensembles, we have computed an NAO index (NAOI) [500 hPa height averaged over ($60°$-$80°N$, $80°W$-$0°E$) subtracted from 500 hPa height averaged over ($30°$-$50°N$, $80°W$-$20°E$)] and a North Pacific index (NPI) [500 hPa height averaged over a domain in the region occupied by the Aleutian low ($30°$-$65°N$, $160°E$-$140°W$)]. These indices are plotted in Fig.8 against the index representing the strength of the tropical SVD1 forcing for the set of ensemble experiments **N_TR**. In Fig.8, the solid (dashed) curve presents the ensemble mean NPI (NAOI), the heavy (light) shading indicates the interval in which the true value of the mean NPI (NAOI) should fall with 95% confidence. The straight solid (dashed)

line shows the NPI (NAOI) derived from the linear model experiment driven by the tropical SVD1 forcing (i.e. Experiment **L_TR**; see Fig.5b). Given the approximately quadratic relationship between the ensemble mean NPI and the strength of the tropical SVD1 forcing, the least-squares linear fit is close to being a flat line, consistent with our previous finding that the linear trend in the suite of experiments **N_TR** underestimates the observed trend over the North Pacific (the much better performance of the linear model is evident from the figure). On the other hand, the quasi-linear relationship between the ensemble mean NAOI and the strength of the SVD1 forcing gives rise to a much steeper slope than its linear counterpart, indicating a somewhat stronger upward trend in the NAOI in the nonlinear experiments than is implied by the linear model. Much of this enhanced upward trend can be attributed to positive feedback from the eddies on the linear wave signal in the North Atlantic sector as noted when discussing Figs. 7c,d.

As a check on the behaviour of the storm track in our model, Fig.9a shows the result of regressing the observed high-band pass filtered variability[4] at 500 hPa against the time series b(t) associated with SVD1 (see Fig.2), and Fig.9b shows the corresponding field derived from an analysis of the high-band pass variability in the nonlinear ensembles driven by global SVD1 forcing with amplitude $\pm$ 1. The amplitude shown in the two figures can be compared directly and shows that the implied trend in high-band pass variability over the Atlantic sector in the model is similar to that observed, but, as expected from our previous discussion, the model behaviour over the North Pacific sector is less realistic. The model nevertheless captures the enhanced storm activity over the North Atlantic that is a feature of the observations (Chang and Fu, 2002).

---

[4]The bimodal filter used here is from Rogers (1997). This filter has maximum response in the frequency range from 2 to 8 days characteristic of synoptic weather systems.

d. Full forcing experiments

So far we have considered the model response (both linear and nonlinear) to forcing by the first SVD mode alone. A question arises as to whether use of the realistic, interannually varying forcing can affect the modeled trend through a nonlinear rectification effect. In fact, we noted earlier that Hoerling et al. (2003) have found that when only the trend in tropical SST is used to drive the NCAR CCM3 model, there is a weakening trend in the Aleutian low, contrary to what is observed and quite different to the deepening trend shown in Hoerling et al. (2001) where the specified tropical SST is the observed monthly mean time series. To investigate the possibility of a rectification effect, we now examine the linear trend in the ensemble mean states produced when the model is run for each winter separately from 1949 to 1999, as in Greatbatch et al. (2003). As can be seen by comparing Fig.10a,b with Fig.6a,b, there is no evidence of a strong rectification effect in the Hall model. Indeed, the linear trend when the full, interannually varying forcing is used to drive the model is very similar to that when SVD1 forcing is used to drive the model. It follows that our model is not capable of shedding light on the rectification mechanism found by Hoerling et al.(2003) in the NCAR CCM3 model. Comparing the modeled trend with the observed trend (Fig.1a), we see that while the spatial features over the North Atlantic and surrounding continents are reasonably well reproduced by the Hall model under globally specified forcing (Expt. **F_G**, Fig.10b), the model overestimates the amplitude of the NAO-like dipole over the North Atlantic and fails to reproduce the deepening trend in the Aleutian low over the North Pacific. A similar impression is gained from the linear trend in Expt. **F_TR**, wherein the model forcing varies from winter to winter only in the tropical band (Fig.10a).

5. Summary and Discussion

This study focuses on the circulation trend in the northern hemisphere winter troposphere during the past 50 years. Pronounced changes took place in both the North Pacific and North Atlantic sectors characterized by a deepening trend in both the Aleutian and Icelandic lows. Here, we began by comparing the 500 hPa circulation patterns associated with (i) the AO; (ii) the linear trend during the last 50 years; (iii) the first northern hemisphere storm activity mode identified by Chang and Fu (2002); (iv) the Cold Ocean Warm Land (COWL) pattern of Wallace et al.(1996) and (v) the leading mode of an SVD analysis based on 500 hPa height and tropical forcing for a dynamical model. The result indicates that the latter four can be grouped under the banner of a "COWL-like" mode which, when compared to the AO, is superior in portraying the recent circulation trend. This "COWL-like" mode manifests the different aspects of the multi-decadal circulation trend including tropospheric warming (note that the COWL index is highly correlated with the time series of the northern hemisphere tropospheric temperature, Wallace et al.,1996), the long-term trend in the northern hemisphere storm track, and the linkage to tropical diabatic processes.

The leading SVD mode (SVD1) of tropical model forcing (which we argued is closely related to the trend in the diabatic forcing of the atmosphere in the tropics) was then applied to drive the dynamical model. The model is a dry, primitive equation model of the atmosphere (the Hall model) that is run in both linear and nonlinear configurations. We began with the version of the model that is linearized about the mean state for all 51 winters 1949-99. The linearized model shows skill in reproducing the observed trend. In particular, when driven by global forcing derived from SVD1, the spatial correlation between the model response and the observations (Fig.2a) is 0.59 (the spatial correlation between the SVD1 pattern shown in Fig.2a and the linear trend shown in Fig.1a is 0.96). Further, the linear model response shows both a deepening trend for the Aleutian low and an upward trend in the NAO index, quite similar to that

observed (the amplitude of the modeled trend is discussed further below). Most of the signal was shown to be captured by restricting the model forcing to the tropics alone, although features over the Eurasian continent are shown to be related to extratropical forcing. The mechanism by which the extratropical circulation feels the tropical diabatic forcing is a planetary wave train that communicates the signal of the changes in the tropics to the extra-tropics. The key region for driving the extratropical planetary wave train is found to be the tropical Indo-Pacific region shown in Fig.2b. Forcing from the western Indo-Pacific (eastern Pacific) is more important for driving the circulation trend over the Pacific and North America (North America and North Atlantic), a picture largely in keeping with Simmons et al. (1983). No role was found for forcing over the tropical Atlantic. All these conclusions have been drawn from the linearized model.

We also described experiments using the nonlinear version of the model. Differences between the linear and nonlinear model results can largely be attributed to the eddy fluxes associated with the model storm tracks. Over the North Atlantic, the eddy fluxes act to reinforce the linear wave signal and enhance the model response, whereas over the North Pacific they act to weaken the deepening trend of the Aleutian low. In fact, in our model, the deepening trend of the Aleutian low is much better captured by the linear model than by its nonlinear counterpart. We also showed that the linear trend in the nonlinear model driven by the complete set of winter to winter varying forcing agrees quite well with the trend obtained from the nonlinear model driven by the SVD1 component of the forcing (essentially the trend in the model forcing). This contrasts with recent results of Hoerling et al. (2003) who found that while the trend over the North Atlantic is captured when the NCAR model is driven only by the trend in tropical SST, running the model with the complete time series of interannually varying SST is required to capture the deepening trend of the Aleutian low. We found no evidence for this nonlinear rectification behaviour in our model. (Note, of course, that the SVD1 diabatic forcing used to drive the Hall model may already contain some

of the rectification effect of the interannually varying SST.)

Hoerling et al. (2003) also argue that the model response over the North Atlantic can be driven by the response of the North Atlantic storm track to remote tropical forcing from the Indian Ocean. Our nonlinear model experiments support this view. As an example, Figure 11 shows the 500 hPa response to SVD1 forcing of magnitude +1 but restricted to only that part of the Indo-Pacific region west of the date line (Experiment **N_WIP** in Table 1). The response of the linearized model to the same forcing is shown in Fig.5e. Comparing Fig.11 with Fig.5e shows very different behaviour in the linear and nonlinear models. Whereas the response of the linear model is confined to the Pacific sector and is characterized by a deepened Aleutian low, the nonlinear model response shows a strong signal over the North Atlantic, characterised by the positive NAO state, and very different behaviour over the North Pacific where a weakened Aleutian low is now found. It follows that, in addition to a linear path, there may also exist a nonlinear path by which the North Atlantic tele-responds to the tropical forcing, the former through a linear planetary wave train and the latter through the adjustment of the North Atlantic storm track to remote tropical forcing. Recently, Branstator (2002) examined the wave-guide effect of the time-averaged tropospheric jets on low-frequency disturbances in the NCAR CCM3 model. He found that the South Asia jet acts as a waveguide that can connect points far apart around the globe, resulting in a circumglobal teleconnection. Moreover, over the North Atlantic, the streamfunction pattern associated with this circumglobal teleconnection has a great deal in common with the structure of the NAO. Therefore, it is conceivable that the wave source over the tropical western Indo-Pacific region can excite perturbations in the South Asia jet, and it is the waveguiding effect of the jet that carries the disturbance to the North Atlantic giving forth to an NAO-like dipole response there. The waveguide mechanism of Branstator (2002) remains a topic for future study.

We commented when discussing the linear model results (Fig.5) that the amplitude

of our model response agrees quite well with the amplitude of the observed circulation trend. This is also generally true of our nonlinear model results, at least over the North Atlantic sector where the forcing associated with the eddy fluxes tends to amplify the linear model response and, in fact, overestimate the amplitude of the observed trend (see Fig.8). In this sense our results differ from Hoerling et al. (2001, 2003) and Hurrell et al. (2003) who found that the NCAR CCM3 model driven by SST forcing can account only for half of the observed amplitude of the trend. Indeed, these authors invoke internal variability of the atmosphere (independent of their specified SST forcing) to explain the remaining half. The reason for this difference in model behaviour is not clear. One reason may be the different ways in which the models are forced. In particular, the forcing used to drive the Hall model is computed directly from observations, whereas in the SST forced experiments of Hoerling et al. the model must compute its own diabatic forcing in response to the specified SST. Our model results suggest that the observed trend can indeed be explained in terms of tropical forcing alone, without the need to invoke internal variability at midlatitudes. The possibility nevertheless exists that the tropical diabatic forcing used to drive our model has, itself, been influenced by internal variability (whether of tropical or extratropical origin). For example, Fedorov et al.(2003) have noted the important role played by unpredictable, midlatitude weather noise in the initiation and subsequent evolution of El Nino events. Future studies using a wide range of models of differing complexity will be required to sort out this issue.

A question naturally arises as to whether the recent circulation trend is part of the natural variability of the climate system, or whether it is driven by anthropogenic forcing or is a combination of both. For example, the 1976-77 climate shift in the Pacific Sector can be understood as a shift in the polarity of the Pacific Decadal Oscillation (PDO), which itself is believed to be an internal mode of variability of the climate system (e.g. Trenberth and Hurrell, 1994; Mantua et al., 1997; Newmann et al., 2003, Deser et al., 2003). The close connection between the recent winter circulation trend

over the northern hemisphere and the 1970's PDO event is supported both by our work and that of Hoerling et al. (2001); in particular, the evidence that the circulation trend was driven by forcing from the tropical Indo-Pacific region. Transitions in the PDO have occurred before, around 1947 and 1925 (Deser et al., 2003), but without any obvious influence on the North Atlantic sector. So, the question arises as to what was different about the event in the 1970's that it had consequences over the whole northern hemisphere, and not just the Pacific sector? Did anthropogenic forcing have some role to play, perhaps through the influence of stratospheric processes on the troposphere (Shindell et al., 1999; Hartmann et al., 2000), or through an anthropogenically forced signal in the tropical SST (Hoerling et al., 2003)?

Concerning the possible importance of anthropogenic forcing, we note that the modelled change in North Atlantic storm activity under SVD1 global forcing of positive amplitude (corresponding to the anomalous forcing during the 1980's and 90's) resembles that found in the ECHAM4/OPYC3 coupled model under increasing greenhouse gas (GHG) forcing (Ulbrich and Christoph, 1999, see their Fig.2). What is not clear, however, is whether the behaviour of the ECHAM4/OPYC3 model is connected with changes in the tropics, such as we have described. We also note that the pattern of tropical Indo-Pacific SST change associated with the trend and shown in Fig.2d is characterized by a warming trend over the tropical Pacific and Indian Oceans that is also similar to the SST fingerprint driven by increased GHG forcing in different coupled models (Meehl and Washington, 1996; Knutson and Manabe, 1998, Hoerling et al., 2003). It is therefore possible that the SVD1 tropical diabatic heating and the associated tropical SST anomalies (and hence also the extratropical response to this heating, including the North Atlantic storm activity change) could be linked to anthropogenic forcing.

Acknowledgments. We are grateful to H. Lin, J. Derome for providing the 51 years

of model forcing computed from the NCAR/NCEP data. We thank Dr. J. M. Wallace for his helpful comment at the formulative stage of this manuscript. We also like to thank two anonymous reviewers for their critical and valuable comments. This work is funded by NSERC, CFCAS and CICS in support of the Canadian CLIVAR Research Network.

References

Branstator, G., 2002: Circumglobal teleconnection, the jet stream waveguide, and the North Atlantic Oscillation, *J. Climate,* **15**, 1893-1910.

Bretherton, C. S., C. Smith and J. M. Wallace, 1992: An intercomparison of methods for finding coupled patterns in climate data, *J. Climate,* **5**, 541-560.

Broccoli, A. J., N.-C. Lau and M. J. Nath, 1998: The Cold Ocean-Warm Land pattern: model simulation and relevance to climate change detection, *J. Climate,* **11**, 2743-2763.

Chang, E. K. M. and Y.-F. Fu, 2002: Interdecadal variability in Northern Hemisphere winter storm track intensity, *J. Climate,* **15**, 642-658.

Christiansen, B., 2003: Evidence for nonlinear climate change: Two stratospheric regimes and a regime shift, *J. Climate* (submitted).

Corti, S., F. Molteni and T. N. Palmer, 1999: Signature of recent climate change in frequencies of natural atmospheric circulation regimes, *Nature,* **398**, 799-802.

D'Andrea F., 2002: Extratropical low-frequency variability as a low-dimensional problem. II: Stationarity and stability of large-scale equilibria, *Quart. J. R. Meteorol. Soc.,* **128**, 1059-1073.

Deser, C., A. S. Phillips and J. W. Hurrell, 2003: Pacific interdecadal climate variability: linkages between the tropics and North Pacific during boreal winter since 1900, *J. Climate,* (submitted).

Fedorov, A. V., S. L. Harper, S. G. Philander, B. Winter and A. Wittenberg, 2003: How predictable is El Niño, *Bull. Am. Meteorol. Soc.*, **84**, 911-919.

Gillett, N. P., H. F. Graf and T. J. Osborn, 2003: The North Atlantic Oscillation. *Climate change and the North Atlantic Oscillation, AGU Geophys. Monogr.*, No. 134, Amer. Goephys. Union, 193-209.

Graham, N. E., 1994: Decadal-scale climate variability in the tropical and North Pacific during the 1970s and 1980s: observations and model results, *Clim. Dyn.,* **10**, 135-162.

Greatbatch, R. J., H. Lin, J. Lu, K. A. Peterson and J. Derome, 2003: Tropical/extratropical forcing of the AO/NAO: A corrigendum, *Geophys. Res. Lett.*, **30**, 10.1029/2003GL017406.

Hall, N. M. J., 2000: A simple GCM based on dry dynamics and constant forcing, *J. Atmos. Sci.,* **57**, 1557-1572.

Hall, N. M. J. and P. D. Sardeshmukh, 1998: Is the time-mean northern hemisphere flow baroclinically unstable? *J. Atmos. Sci.,* **55**, 41-56.

Hartmann, D. L., J. M. Wallace, V. Limpasuvan, D. W. J. Thompson and J. R. Holton, 2000: Can ozone depletion and greenhouse warming interact to produce rapid climate change? *Proc. Nat. Acad. Sci.,* **97**, 1412-1417.

Hilmer, M. and T. Jung, 2000: Evidence for a recent change in the link between the North Atlantic Oscillation and Arctic sea ice export, *Geophys. Res. Lett.*, **27**, 989-992.

Hoerling, M. P. and J. W. Hurrell and T. Xu, 2001: Tropical origin for recent North Atlantic climate change, *Science*, **292**, 90-92.

Hoerling, M. P., J. W. Hurrell, T. Xu, G. T. Bates and A. Phillips, 2003: Twentieth century North Atlantic climate change. Part II: Understanding the effect of Indian Ocean warming, *Clim. Dyn.* (submitted).

Hoskins, B. J. and A. J. Simmons, 1975: A multi-layer spectral model and the semi-implicit method, *Quart. J. R. Met. Soc.,* **101**, 637-655.

Hoskins, B. J. and P. J. Valdes, 1990: On the existence of storm-track, *J. Atmos. Sci.,* **47**, 1854-1864.

Hurrell, J.W., 1995: Decadal trends in the North Atlantic Oscillation: Regional temperatures and precipitation, *Science,* **269**, 676-679.

Hurrell, J.W., 1996: Influence of variations in extratropical wintertime teleconnections on Northern Hemisphere temperature, *Geophys. Res. Lett.*, **23**, 665-668.

Hurrell, J. W., M. P. Hoerling, A. Phillips and T. Xu, 2003: Twentieth century North Atlantic climate change. Part I: Assessing determinism, *Clim. Dyn.* (submitted).

Jin, F.-F. and B. J. Hoskins, 1995: The direct response to tropical heating in a baroclinic atmosphere, *J. Atmos. Sci.,* **52**, 307-319.

Kimoto, M and M. Ghil, 1993: Multiple flow regimes in the northern hemisphere winter. Part I: methodology and hemispheric regimes, *J. Atmos. Sci.*, **50**, 2625-2643.

Kistler, R., W. Collins, S. Saha, G. White, J. Woollen, E. Kalnay, M. Chelliah, W. Ebisuzaki, M. Kanamitsu, V. Kousky, H. van den Dool, R. Jenne, M. Fiorino, 2001: The NCEP-NCAR 50-Year Reanalysis: Monthly Means CD-ROM and Documentation, *Bull. Am. Meteorol. Soc.*, **82**, 247-268.

Knutson, T. R. and S. Manabe, 1998: Model assessment of decadal variability and trends in the tropical Pacific ocean, *J. Climate*, **11**, 2273-2296.

Kumar, A. and M. P. Hoerling, 1998: On the specification of regional SSTs in AGCM simulations, *J. Geophys. Res.*, **103**, 8901-8907.

Lau, N-C., 1997: Interactions between global SST anomalies and the midlatitude atmospheric circulation, *Bull. Am. Meteorol. Soc.*, **78**, 21-33.

Lau, N-C. and M. J. Nath, 1994: A modeling study of the relative roles of tropical and extratropical SST anomalies in the variability of the global atmosphere-ocean system, *J. Climate*, **7**, 1184-1207.

Lau, N-C. and M. J. Nath, 1996: The role of the "atmospheric bridge" in linking tropical Pacific ENSO events to extratropical SST anomalies, *J. Climate*, **9**, 2036-2057.

Lu, J., and R. J. Greatbatch, 2002: The changing relationship between the NAO and northern hemisphere climate variability, *Geophys. Res. Lett.*, **29**, 10.1029/2001GL014052.

Manabe, S., T. R. Knutson, R. J. Stoufeer and T. L. Delworth, 2001: Exploring natural and anthropogenic variation of climate, *Quart. J. R. Met. Soc.,* **127**, 1-24.

Mantua, N. J. and S. R. Hare, Y. Zhang, J. M. Wallace and R. C. Francis 1997, 1997: A Pacific interdecadal climate oscillation with impacts on salmon production, *Bull. Am. Meteorol. Soc.*, **78**, 1069-1079.

McPhaden, M. J. and D. Zhang, 2002: Slowdown of the meridional overturning circulation in the upper Pacific Ocean, *Nature,* **415**, 603-608.

Meehl, G. A. and W. M. Washington, 1996: El Niño-like climate change in a model with increased atmospheric CO_2 concentrations, *Nature,* **382**, 56-60.

Monahan, A. H., L. Pandolfo and J. C. Fyfe, 2001: The preferred structure of variability of the Northern Hemisphere atmospheric circulation, *Geophys. Res. Lett.*, **28**, 1019-1022.

Newman, M., G. P. Compo and M. A. Alexander, 2003: ENAO-forced variability of the Pacific Decadal Oscillation, *J. Climate,* **16**, 3853-3857.

Nitta, T., and S. Yamada, 1989: Recent warming of tropical sea surface temperature and its relationship to the Northern Hemisphere circulation, *J. Meteorol. Soc. of Japan,* **67**, 375-383.

Palmer, T. N., 1999: A nonlinear dynamical perspective on climate prediction, *J. Climate,* **12**, 575-591.

Peterson, K.A., R.J. Greatbatch, J. Lu, H. Lin and J. Derome, 2002: Hindcasting the NAO using diabatic forcing of a simple AGCM, *Geophys. Res. Lett.*, **29**, 10.1029/2001GL014502.

Peterson, K.A., J. Lu, R. J. Greatbatch, 2003: Evidence of the nonlinear dynamics in the eastward shift of the NAO, *Geophys. Res. Lett.*, **30**, 10.1029/2002GL015585.

Rogers, J. C., 1997: North Atlantic storm track variability and its association to the North Atlantic Oscillation and climate variability of Northern Europe, *J. Climate,* **10**, 1635-1647.

Shindell, D. T., R. L. Miller, G. Schmidt and L. Pandofo, 1999: Simulation of recent northern winter climate trends by greenhouse gas forcing, *Nature,* **399**, 452-455.

Simmons, A. J, J. M. Wallace and G. W. Branstator, 1983: Barotropic wave propagation and instability, and atmospheric teleconnection patterns, *J. Atmos. Sci.,* **40**, 1363-1392.

Thompson, D. W. J., J. M. Wallace and G. C. Hegerl, 2000: Annular modes in the extratropical circulation. Part II: Trends, *J. Climate,* **13**, 1018-1036.

Trenberth, K. E., G. W. Branstator, D. Karoly, A. Kumar, N. C. Lau and C. Ropelewski, 1998: Progress during TOGA in understanding and modeling global teleconnections associated with tropical sea surface temperature, *J. Geophys. Res.*, **103**, 14291-14324.

Trenberth, K. E., J. M. Caron, D. P. Stepaniak and S. Worley, 2002: The evolution of ENSO and global atmospheric surface temperatures, *J. Geophys. Res.*, **107**, 10.1029/2000JD000298.

Trenberth, K. E. and T. J. Hoar, 1996: The 1990-1995 El Niño-Southern Oscillation Event: Longest on record, *Geophys. Res. Lett.,* **23**, 57-60.

Trenberth, K. E. and J. W. Hurrell, 1994: Decadal atmospher-ocean interactions in the Pacific, *Clim. Dyn.,* **9**, 303-319.

Ulbrich, U. and M. Christoph, 1999: A shift of the NAO and increasing storm track

activity over Europe due to anthropogenic greenhouse gas forcing, *Clim. Dyn.,* **15**, 551-559.

Wallace, J. M. and D. S. Gutzler, 1981: Teleconnection in the geopotential height field during the Northern Hemisphere winter, *Mon. Wea. Rev.,* **109**, 784-812.

Wallace, J. M., C. Smith and C. S. Bretherton, 1992: Singular value decomposition of wintertime sea surface temperature and 500-mb height anomalies, *J. Climate,* **5**, 561-576.

Wallace, J. M., Y. Zhang and J. A. Renwick, 1995: Dynamical contribution to hemispheric temperature trends. *Science,* **270**, 780-783.

Wallace, J. M., Y. Zhang and L. Bajuk, 1996: Interpretation of interdecadal trends in Northern Hemisphere surface air temperature. *J. Climate,* **9**, 249-259.

Wang, B., 1995: Interdecadal changes in El Niño onset in the last four decades, *J. Climate,* **8**, 267-285.

Wang, B. and S. I. An, 2001: Why the properties of El Niño changed during the late 1970s, *Geophys. Res. Lett.*, **28**, 3709-3712.

Wang, B. and S. I. An, 2002: A mechanism for decadal changes of ENSO behavior: roles of background wind changes, *Clim. Dyn.,* **18**, 475-486.

This manuscript was prepared with the AGU LaTeX macros v3.1.

Table 1. Summary of experiments

	Expt.		
Forcing specification	linear SVD1	Nonlinear SVD1	Full forcing
globe	L_G	N_G	F_G
tropics	L_TR	N_TR	F_TR
extratropics	L_ET	−−	−−
Indo-Pacific	L_IP	−−	−−
West Indo-Pacific	L_WIP	N_WIP	−−
East Pacific	L_EP	−−	−−

Figure 1. Figure 1. (a) The linear trend in 500 hPa height for winters from 1949-1999. Contour interval is 5m/10years; (b) regression of winter mean 500 hPa height against the COWL index. Contour interval equals 10m/1 std of the COWL index.

Figure 2. Figure 2. (a) and (b) show the first pair of dimensional vectors from the SVD analysis on northern hemisphere 500 hPa height and vertically integrated tropical Indo-Pacific forcing for the temperature equation of the Hall model. (a) is the left singular vector for 500 hPa height (contour interval is 10m, the amplitude corresponds to one standard deviation of time series b(t)) and (b) the right singular vector for vertically integrated tropical forcing. (in units of °C/day). (c) shows the standardized expansion coefficients for the first SVD. a(t) is for 500 hPa height and b(t) for the tropical forcing; (d) is the regression of winter mean SST against the time series b(t). Contour interval is 0.1 °C/1 std of b(t).

Figure 3. Figure 3. Time series for indices of NHST1 (top), COWL (middle) and a(t) (bottom). a(t) is the leading SVD expansion coefficient for 500 hPa height. The straight dashed line in each panel denotes the least-squares trend imbedded in the respective time series. The correlation coefficient with a(t) is marked in the top and middle panels, the coefficient for detrended indices being bracketed.

Figure 4. Figure 4. Projection of various 500 hPa height patterns in the subspace spanned by the leading two EOF's. The end point of each colored line is defined by the projection coefficients on the EOF's.

Figure 5. Figure 5. Linear 500 hPa response to SVD1 forcing specified over the whole globe (panel a); the tropics (panel b); the extratropics (panel c); tropical Indo-Pacific ($60°E - 60°W$, panel d); tropical western Indo-Pacific ($60°E - 180°W$, panel e); tropical eastern Pacific ($180°W - 60°W$, panel f). Contour interval is 10m/1 std of b(t) index except in (f) where the contour interval is 5m/1 std.

Figure 6. Figure 6. The linear trend of ensemble mean 500 hPa height in a suite of experiments with the SVD1 forcing increasing from -1.6 to 1.6 at an increment of 0.2. (a) is for tropical SVD1 forcing (Expt. **N_TR**); (b) is for global SVD1 forcing (Expt. **N_G**). Contour interval is 10m/1 std of b(t) index.

Figure 7. Figure 7. (a) and (b) are the response of 500 hPa height in the nonlinear model driven by SVD1 tropical forcing with an amplitude of -1 and $+1$, respectively; (c) and (d) are the linear 500 hPa height response to the diagnosed eddy forcing in the -1 and $+1$ cases, respectively. Contour interval equals 10m/1 std of b(t) index. Note that the patterns displayed in (a) and (c) have been multiplied by -1.

Figure 8. Figure 8. Ensemble mean NPI (solid line symbolized with "+") and NAOI (dashed line symbolized with "+") versus the strength of the tropical SVD1 forcing in Expt. **N_TR**. The breadth of the light (dark) shading indicates the 95% confidence interval (using Student's t-test) for the estimated mean NPI (NAOI). The straight solid (dashed) line shows the variation of NPI (NAOI) with the strength of the tropical SVD1 forcing inferred from the linear experiment **L_TR**. The symbol "$\times$" ("$*$") marks the NPI (NAOI) computed from Fig.2a, i.e. the NPI (NAOI) computed from the observations, for comparison. See the text for the detailed definition of NPI and NAOI and description of experiments **N_TR** and **L_TR**.

Figure 9. Figure 9. (a) The regression of the observed 500 hPa storm track (in terms of root-mean-square of high-pass filtered 500 hPa height) against the time series of b(t); (b) is the average of the response of 500 hPa storm track in the nonlinear model driven by SVD1 global forcing with an amplitude of $+1$ and -1. Note that, before the average, the -1 case has been multiplied by a factor of -1. Contour interval is m/1 std of b(t) index.

Figure 10. Figure 10. The linear trend of ensemble mean 500 hPa height in the nonlinear experiments driven by the full history of tropical (panel a, **F_TR**) and global forcing (panel b, **F_G**). Contour interval is 5m/10years.

Figure 11. Figure 11. The ensemble mean response of 500 hPa height in the nonlinear model driven by SVD1 tropical forcing of amplitude +1 specified over the western Indo-Pacific (between 60°E and 180°W) only. Contour interval is 10m/1 std of b(t).

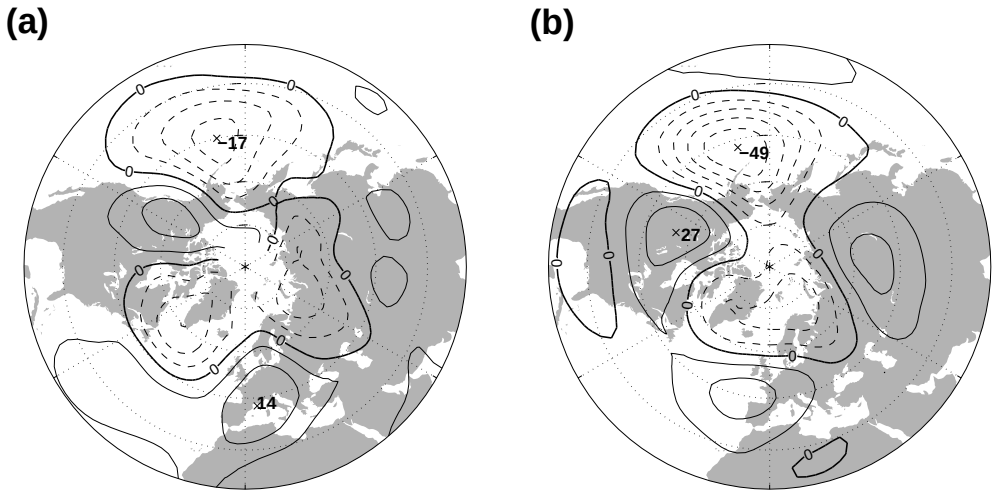

Figure 1. (a) The linear trend in 500 hPa height for winters from 1949-1999. Contour interval is 5m/10years; (b) regression of winter mean 500 hPa height against the COWL index. Contour interval equals 10m/1 std of the COWL index.

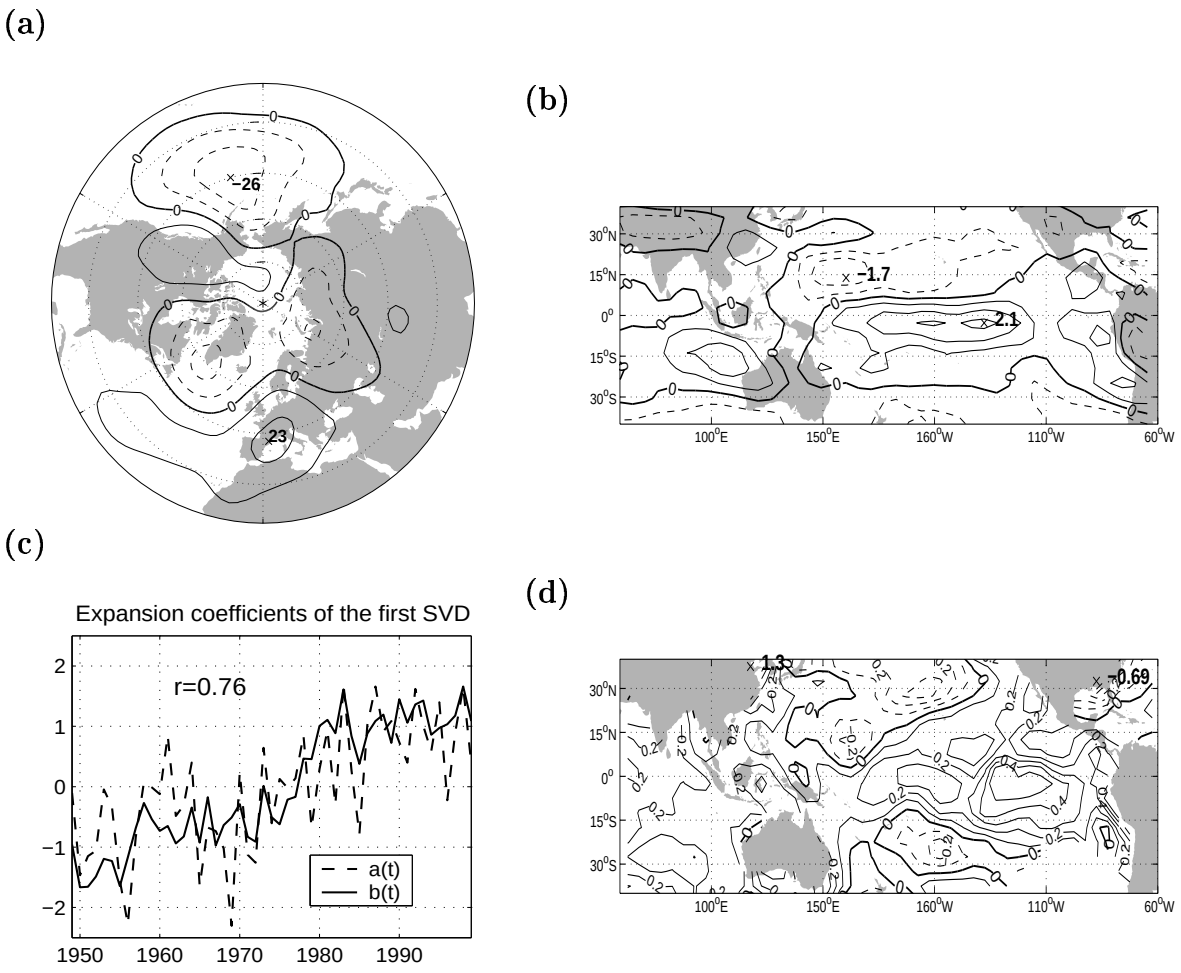

Figure 2. (a) and (b) show the first pair of dimensional vectors from the SVD analysis on northern hemisphere 500 hPa height and vertically integrated tropical Indo-Pacific forcing for the temperature equation of the Hall model. (a) is the left singular vector for 500 hPa height (contour interval is 10m, the amplitude corresponds to one standard deviation of time series b(t)) and (b) the right singular vector for vertically integrated tropical forcing (in units of °C/day). (c) shows the standardized expansion coefficients for the first SVD. a(t) is for 500 hPa height and b(t) for the tropical forcing; (d) is the regression of winter mean SST against the time series b(t). Contour interval is 0.1 °C/1 std of b(t).

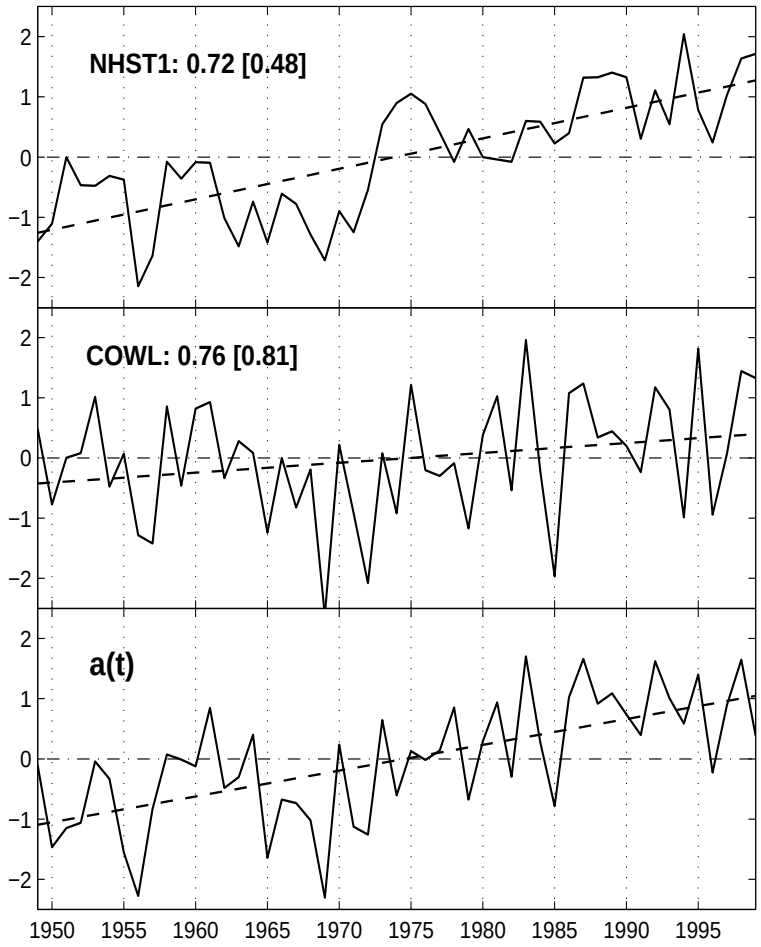

Figure 3. Time series for indices of NHST1 (top), COWL (middle) and a(t) (bottom). a(t) is the leading SVD expansion coefficient for 500 hPa height. The straight dashed line in each panel denotes the least-squares trend imbedded in the respective time series. The correlation coefficient with a(t) is marked in the top and middle panels, the coefficient for detrended indices being bracketed.

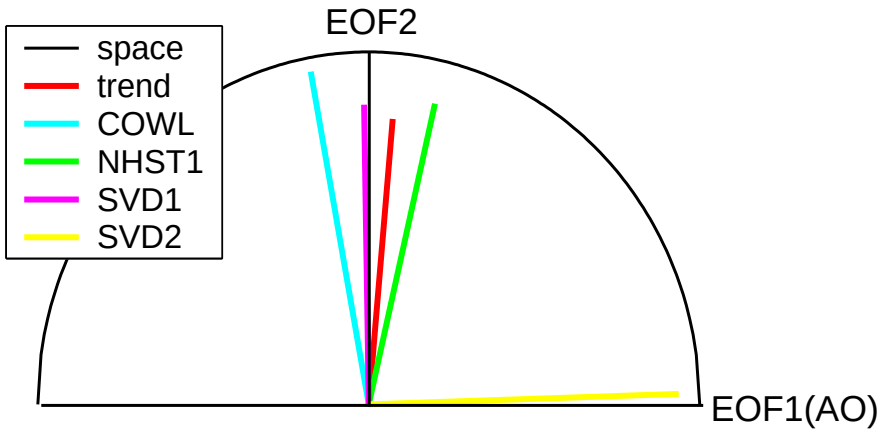

Figure 4. Projection of various 500 hPa height patterns in the subspace spanned by the leading two EOF's. The end point of each colored line is defined by the projection coefficients on the EOF's.

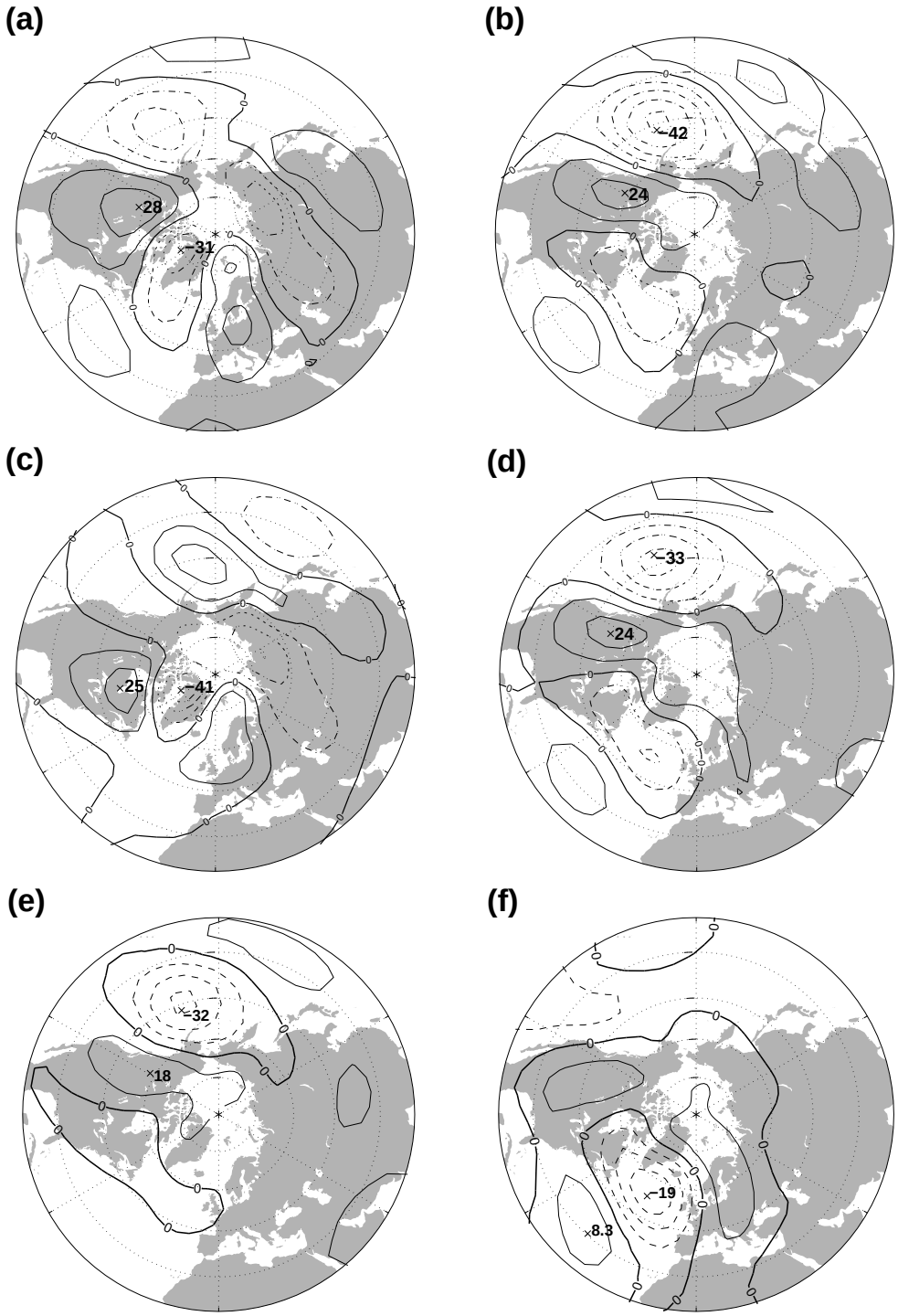

Figure 5. Linear 500 hPa response to SVD1 forcing specified over the whole globe (panel a); the tropics (panel b); the extratropics (panel c); tropical Indo-Pacific ($60°E - 60°W$, panel d); tropical western Indo-Pacific ($60°E - 180°W$, panel e); tropical eastern Pacific

($180°W - 60°W$, panel f). Contour interval is 10m/1 std of b(t) index except in (f) where the contour interval is 5m/1 std.

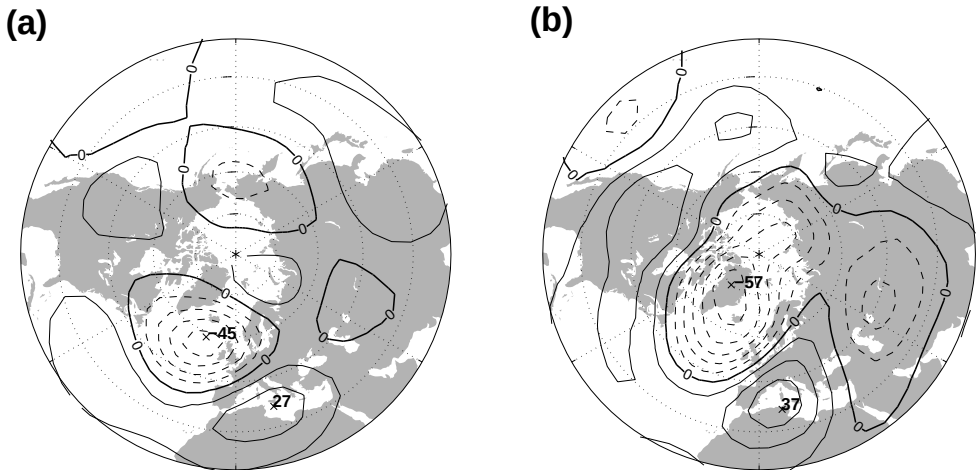

Figure 6. The linear trend of ensemble mean 500 hPa height in a suite of experiments with the SVD1 forcing increasing from -1.6 to 1.6 at an increment of 0.2. (a) is for tropical SVD1 forcing (Expt. **N_TR**); (b) is for global SVD1 forcing (Expt. **N_G**). Contour interval is 10m/1 std of b(t) index.

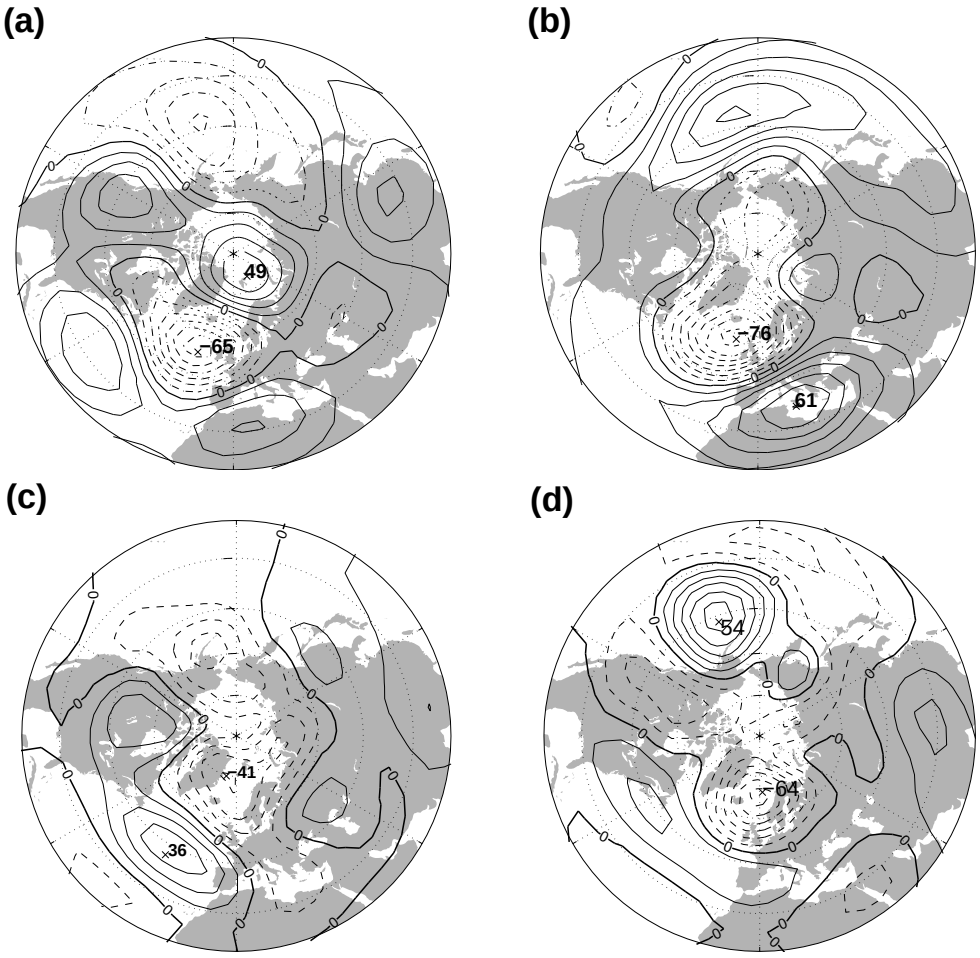

Figure 7. (a) and (b) are the response of 500 hPa height in the nonlinear model driven by SVD1 tropical forcing with an amplitude of -1 and $+1$, respectively; (c) and (d) are the linear 500 hPa height response to the diagnosed eddy forcing in the -1 and $+1$ cases, respectively. Contour interval equals 10m/1 std of b(t) index. Note that the patterns displayed in (a) and (c) have been multiplied by -1.

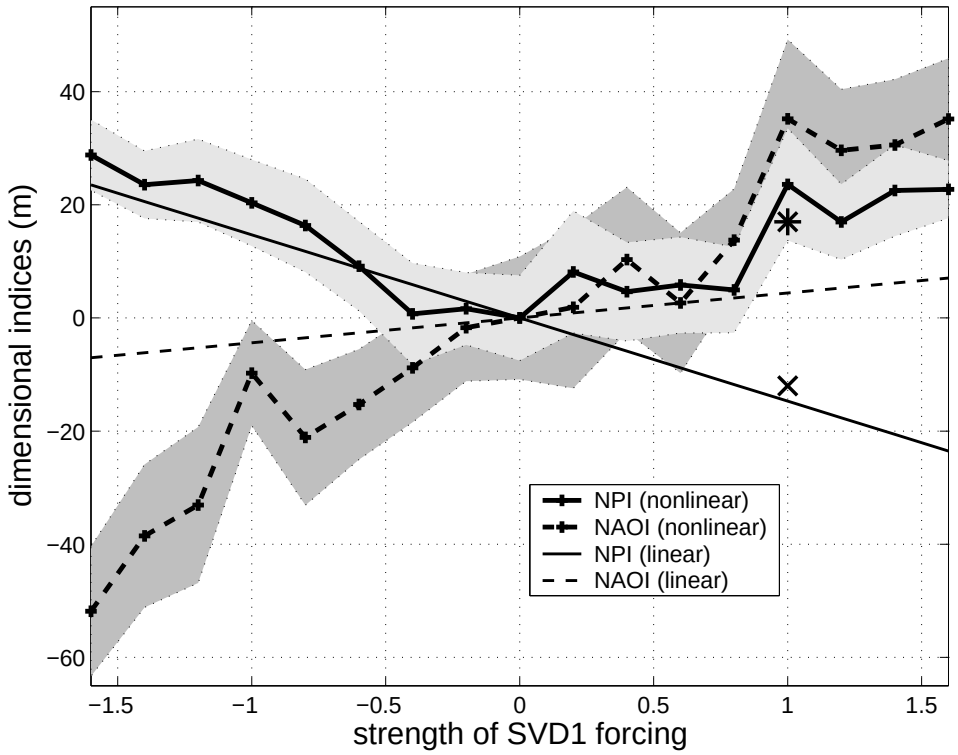

Figure 8. Ensemble mean NPI (solid line symbolized with "+") and NAOI (dashed line symbolized with "+") versus the strength of the tropical SVD1 forcing in Expt. **N_TR**. The breadth of the light (dark) shading indicates the 95% confidence interval (using Student's t-test) for the estimated mean NPI (NAOI). The straight solid (dashed) line shows the variation of NPI (NAOI) with the strength of the tropical SVD1 forcing inferred from the linear experiment **L_TR**. The symbol "×" ("∗") marks the NPI (NAOI) computed from Fig. 2a, i.e. the NPI (NAOI) computed from the observations, for comparison. See the text for the detailed definition of NPI and NAOI and description of experiments **N_TR** and **L_TR**.

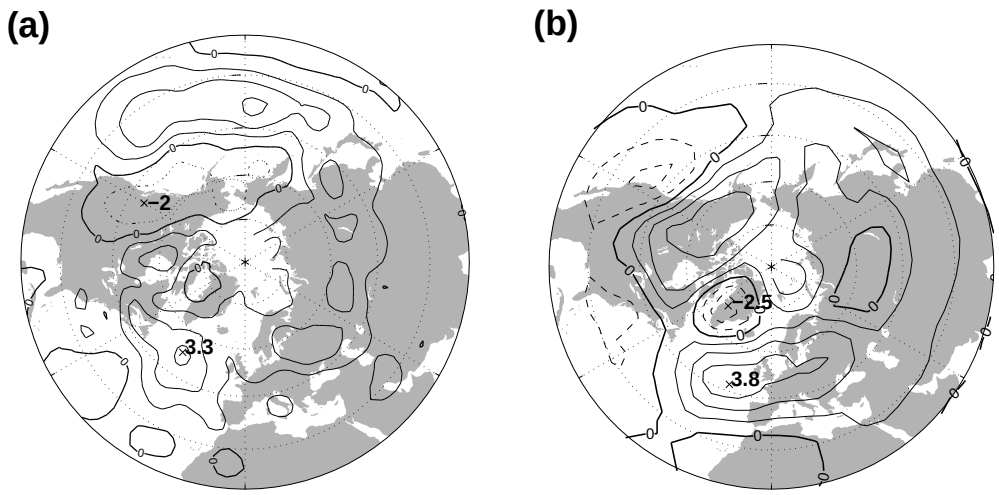

Figure 9. (a) The regression of the observed 500 hPa storm track (in terms of root-mean-square of high-pass filtered 500 hPa height) against the time series of b(t); (b) is the average of the response of 500 hPa storm track in the nonlinear model driven by SVD1 global forcing with an amplitude of +1 and −1. Note that, before the average, the −1 case has been multiplied by a factor of −1. Contour interval is m/1 std of b(t) index.

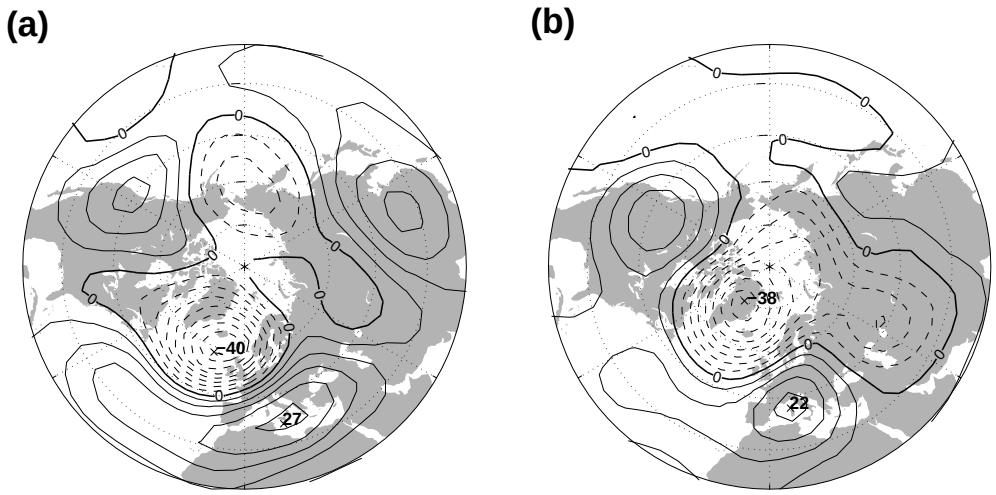

Figure 10. The linear trend of ensemble mean 500 hPa height in the nonlinear experiments driven by the full history of tropical (panel a, **F_TR**) and global forcing (panel b, **F_G**). Contour interval is 5m/10years.

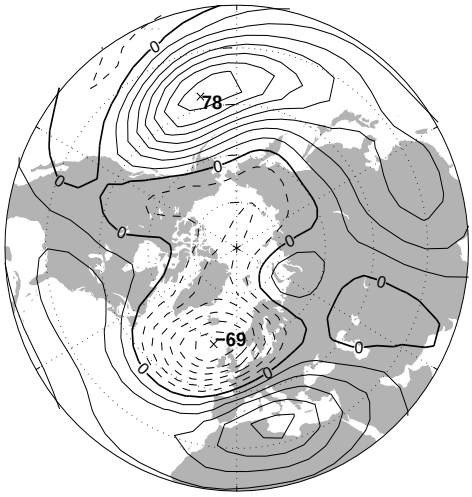

Figure 11. The ensemble mean response of 500 hPa height in the nonlinear model driven by SVD1 tropical forcing of amplitude +1 specified over the western Indo-Pacific (between 60°E and 180°W) only. Contour interval is 10m/1 std of b(t).